CORE
Metadata, citation and similar papers at core.ac.uk
Provided by University of Strathclyde Institutional Repository

Fault Location and Diagnosis in a Medium Voltage EPR Power Cable

A. J. Reid, C. Zhou and D. M. Hepburn
School of Engineering and Built Environment
Glasgow Caledonian University
Glasgow, G4 0BA, UK

M. D. Judd and W. H. Siew
Institute for Energy and Environment
University of Strathclyde
Glasgow, G1 1XW, UK

P. Withers
Manchester X-ray Imaging Facility
Materials Science Centre
University of Manchester, M13 9PL, UK

ABSTRACT

This paper presents a case study on fault location, characterisation and diagnosis in a length of shielded 11 kV medium voltage ethylene-propylene rubber (EPR) power cable. The defect was identified on-site as a low resistance fault occurring between the sheath and the core. A 43 m section was removed for further analysis. The fault resistance was characterised and the location of the defect pinpointed to within a few cm using a combination of time-difference-of-arrival location and infra-red imaging. A combination of X-ray computed tomography, scanning electron microscopy and energy dispersive X-ray spectroscopy were then applied to characterise any abnormalities in the dielectric surrounding the breakdown region. A significant number of high density contaminants were found to be embedded in the dielectric layer, having an average diameter of the order of 100 μm, a maximum diameter of 310 μm and an average density of 1 particle per 2.28 mm^3. Scanning electron microscopy and energy-dispersive X-ray spectroscopy were used to determine the geometry and elemental composition of some initial contaminant samples. It was concluded that contamination of the EPR layer, combined with an observed eccentricity of the cable's core and sheath resulting in a reduced insulation gap, may have led to an electric field concentration in the region of the defect sufficient to initiate breakdown. Preventative strategies are discussed for similar families of cables, including more stringent dielectric testing requirements at the manufacturing stage and PD monitoring to detect incipient failure.

Index Terms — **Power cable insulation, power system faults, condition monitoring, dielectric breakdown.**

1 INTRODUCTION

POWER cables form an integral part of power generation, transmission and distribution systems. With an increasing rate of failure due to ageing and operational stresses, maintaining the integrity of a cable network through effective monitoring and replacement is a subject of importance today. Understanding the characteristics, location strategies and underlying causes of a cable fault can be effective in informing monitoring and replacement schemes for such assets in the future. In many cases, preventative maintenance through the use of on-line partial discharge (PD) monitoring can allow an incipient fault to be detected and located before an eventual failure occurs [1]–[4]. If the initial defect is not detected in its incipient stages, it may increase in severity, eventually leading to complete breakdown. Increased defect severity may be characterised by, for example, a change in resistivity, a break in the conductors or by partial bridging of the insulation. Various approaches to defect location [5] have been developed over the years with each method having its own relative merits. The severity of such defects often

precludes the application of partial discharge monitoring.

The aim of this case study was firstly to apply an effective post-fault location technique in the lab to pinpoint the fault on a length of cable that has been taken out of service. Secondly, the study aims to characterise the geometric detail of the region surrounding the fault through the application of X-ray and microscopy techniques, allowing a hypothesis to be proposed for the initial cause of breakdown. It is suggested that the reported measurements on a medium voltage EPR cable, of the type commonly used in power generation, will inform improved future PD monitoring and testing strategies, leading to a reduced failure rate in generation networks of this type.

1.1 THE CABLE SAMPLE

The cable was single phase EPR, rated at 11 kV. A length of 43 m was removed and taken out of service after the occurrence of a breakdown and transferred to the laboratory for further testing. The section under examination was manufactured in 1983 to standard BS6622 [6] and has been in service from this date until the breakdown occurred in 2009. The cable had a single core stranded compacted aluminium inner conductor, stripable semiconducting screen, EPR dielectric, wound copper tape outer conductor, PVC bedding, aluminium wire armour and a PVC outer sheath with reduced flame propagation characteristics. No PD monitoring was previously applied on site (although PD may have initially occurred before breakdown). During operation, the defect increased in severity forming a partially-conductive channel through the insulation layer. This precluded PD-based location techniques. The following sections will describe an investigation of the fault characteristics, detailing the location methods applied and the accuracy of these methods in this case.

2 DEFECT LOCATION

2.1 INITIAL DIAGNOSIS

Initial tests aimed to determine the defect type. These were first carried out using an insulation resistance testing device to investigate any discrepancies in the core, sheath and insulation resistances. No abnormalities were found in the conductors, but the resistance between outer and inner conductor was found to vary between 1 - 10 MΩ at an applied voltage of 500 V rms, indicating a possible shunt resistance defect. Results of fault resistance measurement were not repeatable, varying by several MΩ on each occasion. The cable was next tested at operational voltage. PD-free terminations at each end were necessary in order to prevent spurious discharges from interfering with subsequent time-difference-of-arrival (TDOA) measurements. These were constructed using pre-moulded stress cones. The application of a ramped ac voltage revealed that the fault underwent transition from a high to a low resistance, manifested by a single transient waveform generating sufficient current to be extracted using two high frequency current transformers (HFCTs) at each cable end. The comparatively low resistance of the shunt defect allowed Joule heating of the channel to be used as a means of confirming or otherwise, TDOA location accuracy.

2.2 TIME-DIFFERENCE-OF-ARRIVAL MEASUREMENT

Figure 1 shows the experimental setup for TDOA location. The TDOA location technique has been a subject of interest in overhead power line research [7]–[9]. For example, Bo et al [10] have applied this method to overhead power lines and suggested it can be applied to underground power cables. In this case the cable was connected to the output of a 50 kV transformer with the voltage applied between the core and sheath. The supply voltage V_s was increased until transition from a high to a low resistance occurred in the fault channel. The resulting single fast transient current pulse was extracted at each cable end by positioning two HFCTs the earth straps, as shown in Figure 1. Each HFCT had a sensitivity of 5 V/A in the operational range 5 kHz - 10 MHz.

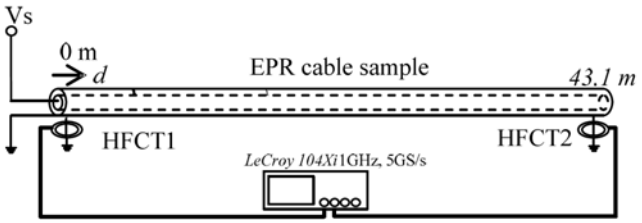

Figure 1. Experimental setup for TDOA location of breakdown pulse from cable fault.

Knowledge of the propagation velocity u_p of a transient electromagnetic wave in the EPR medium was necessary for time-of-flight calculations. Due to dispersion effects, u_p varies with frequency. It was therefore necessary to determine the propagation velocity of transverse electromagnetic waves in the coaxial transmission line formed by the cable in the expected frequency range of electromagnetic radiation emanating from a typical breakdown current pulse. To determine u_p, the experimental setup shown in Figure 2 was used.

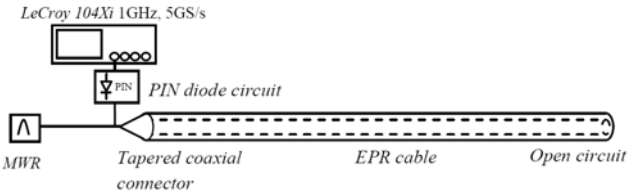

Figure 2. Experimental setup for measurement of propagation velocity u_p.

Injection of repetitive pulses in the appropriate frequency range was achieved using a mercury wetted relay (MWR) device. This allowed fast switching of high amplitude pulses in a nanosecond timescale, producing similar waveforms to those observed as a result of cable breakdown. Both the initial injected pulse and the pulse reflected from the open circuit end of the cable were captured using a non-linear attenuator

circuit based on PIN diodes, as shown in Figure 2. This novel approach protected the oscilloscope's input voltage from the initial high amplitude injected pulse, while still allowing the low amplitude reflected pulse to be measured with high sensitivity. The time difference between injected and reflected pulses was 581 ns, corresponding to twice the transit time of the cable. Since the exact physical length of the cable could be measured, u_p could be calculated using the equation $u_p = l / \Delta T$ where l is the physical length of the cable and T is transit time along its length. In this case, $u_p = 43.1/290.5 \times 10^{-9} = 1.48 \times 10^8$ ms^{-1}.

The measurement error in time difference was estimated to be ±4 ns, caused by limitation of the scope's horizontal resolution combined with the error in estimating the starting point of the reflected pulse's rising edge due to dispersion effects.

Variation in the conductivity of the fault was evidenced by a fluctuation in the voltage across the cable, with the peak of the supply voltage occasionally clipping as the fault channel underwent quasi-breakdown at high amplitudes. At this transition point it was possible to observe low amplitude emitted transients. An example is shown in Figure 3.

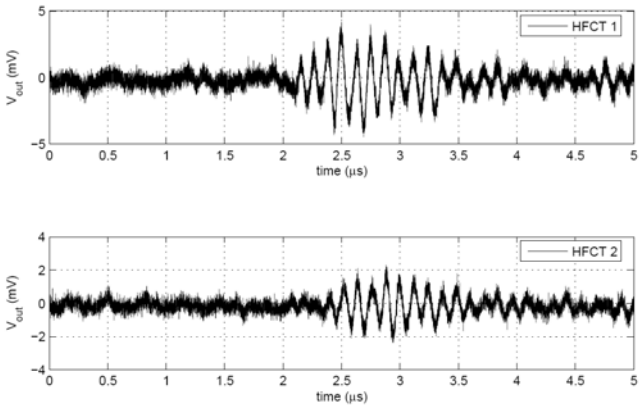

Figure 3. Measured traces at the respective HFCTs arising from breakdown at the site of the cable fault. Δt = 261 ns.

Fault location was then calculated using the equation:

$$d = \frac{l - \Delta t \cdot u_p}{2} \qquad (1)$$

where Δt is the time-difference-of-arrival between measured signals at HFCTs 1 and 2. This was achieved by identifying similar features on the respective waveforms arriving at each HFCT, such as the initial peaks, and estimating the time difference between these features. Taking into account measurement errors in Δt and ΔT, the signals shown in Figure 3 correspond to a fault location of d = 2.18 ± 0.56 m from HFCT1 (see Figure 1).

2.3 THERMAL LOCATION

To verify the accuracy of the above results, thermal location was next applied. Energy dissipated by the fault current was sufficient to raise the surrounding region above ambient temperature. A thermal imaging camera (FLIR E45) with a temperature resolution of 0.1°C was used pinpoint the location to within a few cm.

The cable was energised for 15 minutes at a maximum applied voltage of 35 V rms. This relatively low value was due to the shunt fault forming a low resistance channel to earth, reducing the potential difference between core and sheath. Thermal imaging revealed the location of the shunt fault to be 1.8 m from the cable end. This falls within the measurement error of the previous location result, confirming the accuracy of the applied TDOA method. Figure 4 shows a thermal image of the energised cable overlayed on a photograph of the same planometric view of the cable layout.

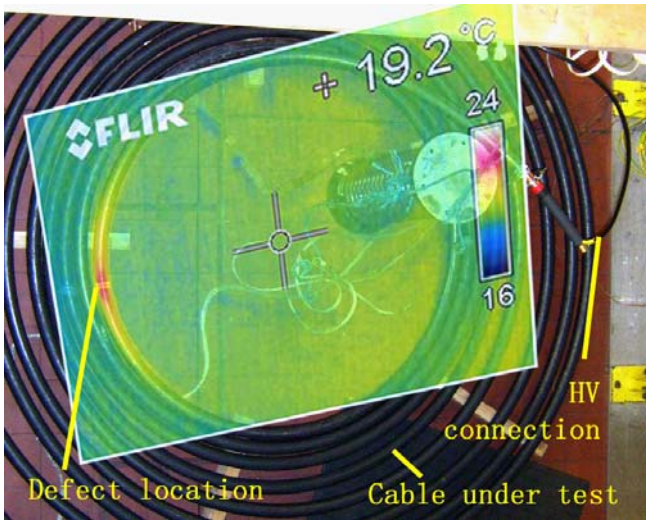

Figure 4. Fault location using infra red imaging. The location is 1.8 m from the cable datum end. For clarity, this composite image consists of the thermal image superimposed on a photograph of the experimental setup.

The cable had been placed in a spiral arrangement so that the entire cable length was within the field of view. The site of the fault was apparent on the inner coil of the spiral arrangement as evidenced by increased temperature in the region. Once thermal equilibrium was reached the peak cable temperature was found to be 21.7°C (2.5°C above the ambient level).

It was of interest to characterise parameters of the fault. For example, since the cable voltage, current and phase could be measured, fault resistance could be evaluated in terms of its variation with applied voltage. The resistance of the active fault region is related to its reflection coefficient. Knowledge of this resistance is therefore useful in determining the accuracy of reflection-based location methods. This will be discussed further in the next section.

3 DEFECT ANALYSIS

3.1 CHARACTERISATION OF RESISTANCE

The voltage across and current through the cable were measured as indicated in Figure 5, where, I_p is the primary current, I_s is the secondary current, V_s is the secondary voltage and C_{cable} is the capacitance of the cable under test from inner to outer conductor.

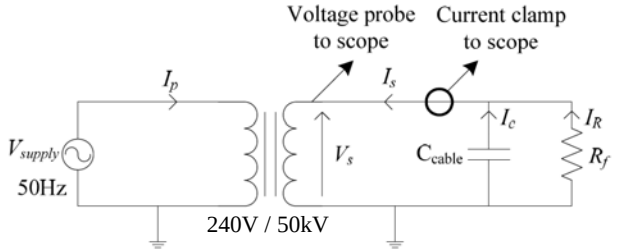

Figure 5. Experimental setup for measurement of fault resistance R_f of the conductive channel between core and sheath.

The real part of the secondary current was calculated from the phasor diagram in Figure 6 using the equation:

$$I_R = \cos(\delta) \cdot I_s \quad (2)$$

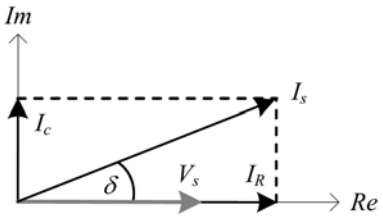

Figure 6. Phase relationship between voltages and currents in the measurement set up of Figure 5.

The fault resistance was calculated by dividing the secondary voltage by I_R. Four different tests were carried out to check repeatability. Due to the limitation in current which could be drawn from the LV supply (around 16 A), the maximum voltage that could be applied to the cable was around 35 V rms at the point where the defect resistance had reached a steady-state value. Figure 7 shows the variation in the fault resistance measurements for four repeated experiments.

Due to the capacitive impedance of the cable, a phase difference existed between the secondary current and secondary voltage, with the current leading the voltage by an angle between 0^o and 90^o, depending on the value of fault resistance R_f. Calculation of the fault resistance required the real part of the secondary current to be known. It was therefore necessary to measure the phase difference between V_s and I_s. It was found that the capacitive impedance of the cable dominated, having an approximate value of 200 kΩ and that the phase difference was small (~$5^{o,}$), especially at higher applied voltages. Fault resistance fluctuated between 2 kΩ and 6.5 kΩ at the minimum applied voltage. The variation in fault resistance was plotted against the voltage across the cable (test object). This is shown in Figure 7.

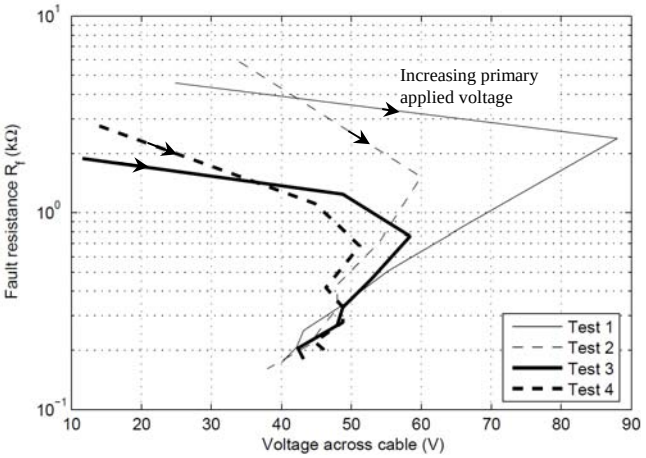

Figure 7. Variation of fault resistance with the voltage across the cable.

Arrows shown in the figure indicate an increasing supply voltage (and current) applied at the primary winding. In each of the four tests, a corresponding increase occurs in the voltage across the cable, until the fault reaches a transition point where its resistance decreases significantly. In each of the test cases, the defect resistance approaches a minimum of around 200 Ω at the maximum applied primary voltage. This minimum value was consistent with that initially obtained by the site engineer, leading to decommissioning of the cable.

3.2 PHYSICAL INSPECTION

A short cable section of approximate length 200 mm was removed at the location of the suspected fault. With the outer sheath and aluminium wire armour removed, visible damage was found at a location corresponding to 1.8 m from the cable end nearest HFCT1. This confirmed thermal and TDOA location accuracy to within a few cm. Carbonised tracking was evident around the perimeter of a 3 mm occlusion at the site of the breakdown. It was proposed that the internal structure would be revealed in further detail by means of X-ray computed tomography. This is described in the following section.

3.3 X-RAY COMPUTED TOMOGRAPHY

The aim of the analysis was to capture internal geometric detail of the fault and surrounding medium. X-ray computed tomography (or computed axial tomography) is ideally suited to this purpose. In this method, the sample is rotated axially, with an X-ray image taken at each small increment in rotation of the test object. On completion of the X-ray process digital geometric processing is applied to the acquired images in order to reconstruct the sample into a 3-dimensional digital representation of the volume. This approach is highly advantageous as it allows for non-destructive analysis of the fault.

The X-ray scanner used in this study was a Nikon custom static bay with a 225 kV multi-metal anode source. The samples were positioned between the X-ray source and a 2k by 2k Perkin Elmer 1621 XRD 16-bit amorphous silicon flat panel detector, allowing images to be captured in high detail.

Several factors had to be considered when determining the feasibility of X-ray imaging of the sample. Firstly, an appropriate beam energy spectrum had to be chosen. Unlike biological samples which are commonly analyzed using X-ray computed tomography techniques, scanning of the cable is challenging in that the beam must simultaneously have high enough energy to penetrate through the conductive sections and be detected by the receiver, whilst still allowing the subtle internal features of the low density EPR layer to be captured in high detail. After initial trials it was found that a Molybdenium (Mo) anode source was most effective in producing an appropriate photon energy spectrum to clearly identify all internal features of the samples.

Secondly, it was desirable to achieve as fine a spatial resolution as possible. In the present setup, X-ray resolution was limited by the sample size due to the relative positions of the source, sample and detector array. The sample was placed as close as possible to the X-ray source. The beam was emitted from the point source, passing through the sample, and then detected by a flat panel array of around 0.5 m^2. The closer the test object can be placed to the source, the greater the spatial resolution of the captured images on the detector. An analogy here is that of a lamp projecting a shadow onto a wall; the closer an object is placed to the lamp, the finer the spatial resolution of the shadow that it casts. In the case of the cable, which has a diameter of 30.5 mm with the outer conductor removed, points on the sample could be positioned a maximum distance of 30.5 mm from the X-ray source. This led to a minimum achievable resolution of 18.3 μm. Test were initially carried out using the full cable sample, giving geometric details at the above resolution. To achieve finer resolution, a small slice of the insulating layer was removed, allowing it to be rotated in front of the beam at a distance of less than 15 mm. This allowed internal details of the EPR slice to be viewed with a greatly improved minimum resolution of 9 μm.

The third consideration in the feasibility of testing was tomographic reconstruction of the data. The geometry of the object plays an important role. Fortunately, the quasi-isotropic cable geometry lends itself ideally to volumetric reconstruction of a series of images around the cable's central axis. This was because the reconstruction software was able to easily identify common highly contrasting features of consecutive images such as the outer edges of the aluminium core and EPR layer. The data could therefore be reconstructed with a high degree of accuracy.

Initially, the cable sample was scanned with the inner conductor, semicon and EPR layers intact. It was found that the following settings achieved the optimal contrast on acquired images: Acquisition time = 1.4 seconds; Applied voltage = 110 kV; Applied X-ray current = 85 μA. The total size of the raw images was around 20 GB. Since images were reconstructed at the maximum possible resolution, the reconstructed volumes were around 50-100 GB is size and required intensive graphical and computational processing to plot. Fig. 8 shows a reconstructed orthographic slice on a plane normal to the cable's longitudinal axis.

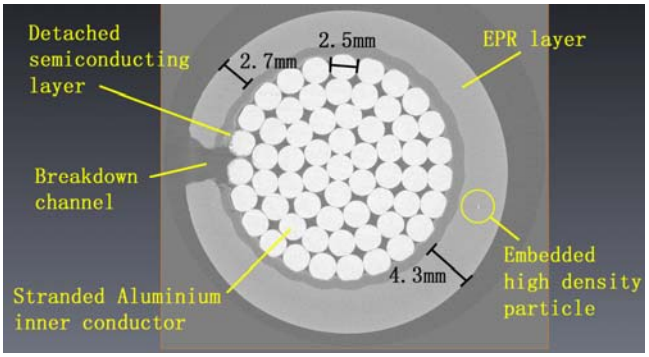

Figure 8. Reconstructed X-ray slice through defective cable section showing breakdown channel and conducting particle contaminant.

Several features are immediately evident. Firstly, the breakdown channel is clearly visible, having a diameter of 2-3 mm. Tracking caused by the breakdown current has extensively degraded the dielectric so that the channel is essentially an air gap at this stage. Secondly, the breakdown has caused the inner semiconductor to detach from the inner conductor leaving a cavity. Thirdly, eccentricity is evident, with a 1 mm offset between the longitudinal central axes of the aluminium stranded core and the EPR insulation layer, resulting in an increased insulation gap on one side of the cable and a reduced insulation gap on the other. Fourthly, the presence of at least one high-density particle with an approximate diameter of 100 μm is evidently embedded within the insulation layer. The particle appears to have a similar density to that of the aluminium core. The appearance of the particle on this arbitrary cross section suggests a possible high contaminant density in this region.

Fig. 9 shows the results of volume rendering of the reconstructed data. Rendering the high-density region as an isosurface, while separately rendering the volume of the EPR and semiconducting layers, allowed the effect of artificially removing the insulation layer. This revealed the presence of multiple high-density contaminants. Several contaminants have been highlighted in Fig. 9 (c) for illustration purposes. Damage to the inner core is evident around the breakdown region as is an increased contaminant density. Due to sustained stressing, the fault has largely disintegrated the EPR region surrounding it. Particle diameters are of the order of 100 μm.

At this stage it was likely that the maximum resolution of the measurement system was imposing a limit on the visible internal details of the insulation layer. As mentioned

previously the size of the sample imposes a lower limit on the imaging resolution of the X-ray system and consequently, the smallest resolvable detail of the sample. A thin slice of EPR was therefore removed from the cable and analyzed separately. This achieved an improved minimum resolution of 9 μm. Results are shown in Figs. 10 and 11. It can be seen from the 2D orthographic view of Fig. 11 that more contaminants are now visible, with diameters ranging from 40 μm to 300 μm. Note that the bright regions near the edges of the sample are not due to increased material density but are an artifact of the geometric reconstruction algorithm.

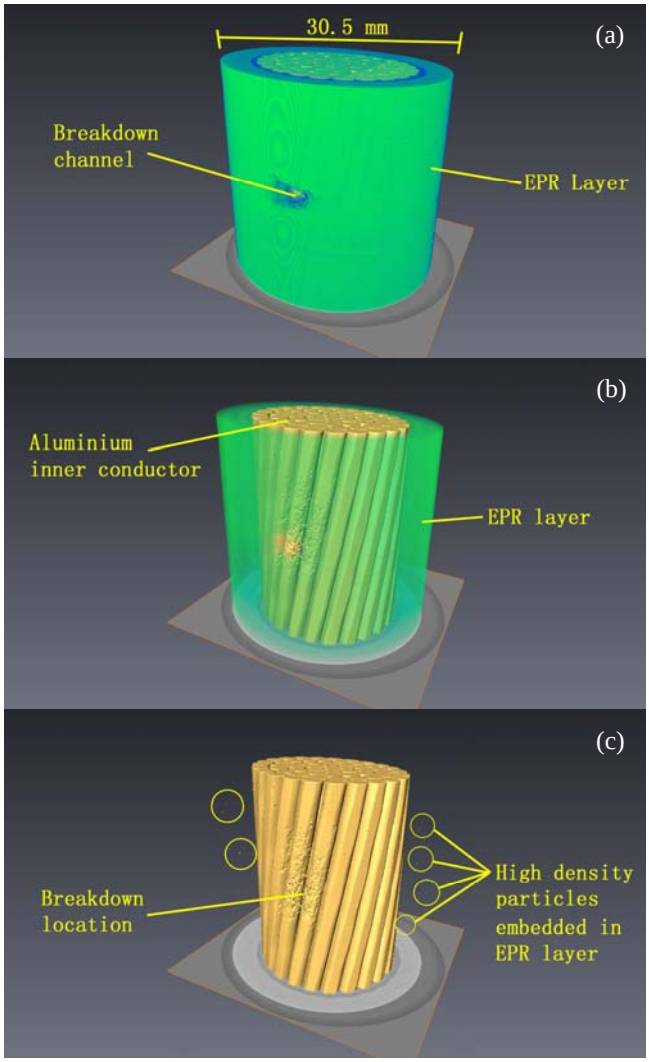

Figure 9. Reconstructed cable geometry from X-ray scans. (a) EPR layer is fully visible, (b) EPR layer set to semi-transparent, (c) EPR layer hidden to show particle contamination and damage to inner conductor.

Fig. 11 shows the reconstructed volume of the small dielectric sample. Setting the low-density insulation region as a semitransparent layer reveals the embedded contaminants. The average particle density in this region is 1 particle per 2.28 mm^3.

The above results show a non-destructive method of obtaining the internal geometrical characteristics of the breakdown region and insulation layer, revealing details of high-density contaminants with a resolution of 9 μm. The following sections present the results of additional analysis using scanning electron microscopy and spectroscopy techniques to reveal more detailed geometric detail and elemental composition of the cable sample.

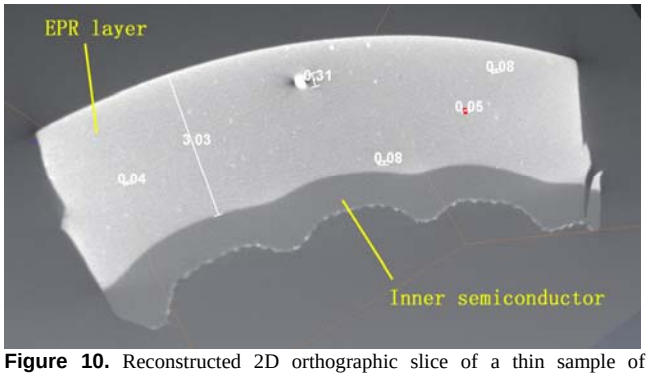

Figure 10. Reconstructed 2D orthographic slice of a thin sample of insulator near the defect region. Embedded high density particles appear as light regions. Dimensions are in mm.

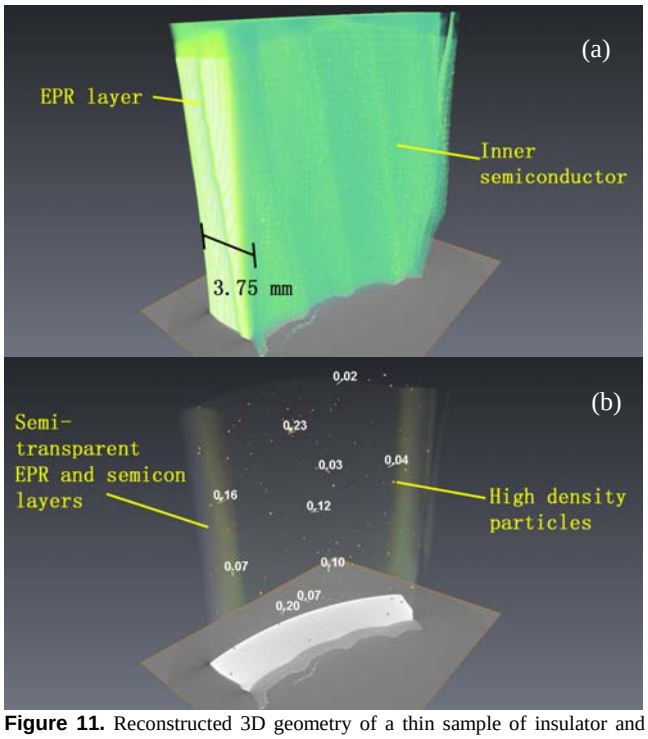

Figure 11. Reconstructed 3D geometry of a thin sample of insulator and semiconductor removed from near the defect region. (a) Semiconducting and EPR layers fully visible, (b) EPR and semiconducting layers set semitransparent to reveal embedded high density particles. Dimensions in mm.

3.4 SCANNING ELECTRON MICROSCOPY

Computer aided X-ray tomography has revealed geometrical detail down to a μm resolution. Detected contaminants appear to have a density similar to that of

Aluminium. Investigation of whether the observed particles may be the source of the breakdown requires further analysis. Specifically, finite element modeling should allow the degree to which the electric field enhancement in the region is likely to induce breakdown.

In this case, an EDAX Evo 50 system was used, allowing geometric details to be resolved at a sub-micron resolution. With a maximum magnification of 1,000,000x, features down to 2 nm could be resolved. The only disadvantage was the destructive nature of the method; it was necessary to physically cut the insulation material, since it is only possible to scan the surface of a material. This meant that the probability of finding an anomalous particle on the surface of a sample decreased significantly compared to the previous technique.

The test procedure was as follows: Firstly a few, thin EPR samples with a surface area of a few mm^2 were cut from the EPR layer using a scalpel. For SEM microscopy to be effective the samples must be conducting. Charge buildup will manifest itself as high brightness regions, distorting the micrograph image. Clearly, EPR is an insulating material particularly effective at storing charge. Prior to scanning, therefore, it was necessary to gold-plate each sample to a thickness of a few atoms. A standard Kimball filament was used as the SEM electron source. With the chamber evacuated and the sample correctly positioned, it was found that a probe current of 10 pA and an applied voltage of 15-20 kV produced the best images. One of the initial results is shown in Fig. 12. The embedded particle is clearly visible with more details of the geometry now evident compared with the previous X-ray images. The particle shape is typical of those encountered in other SEM micrographs, having flat regions and several sharp edges.

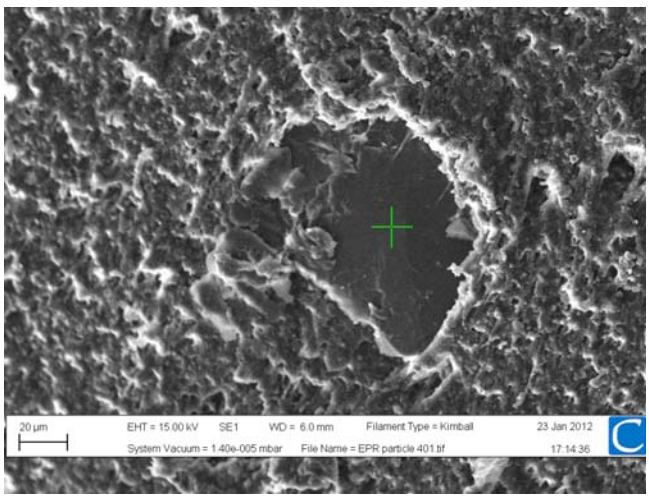

Figure 12. SEM micrograph of a sliced surface of EPR insulating material from the cable sample showing an embedded high density particle.

3.5 ENERGY DISPERSIVE X-RAY SPECTROSCOPY

Based on results of the previous sections, the elemental composition of the contaminants may only be assumed on the basis of apparent density as it appears in the X-rays. Computation of electric field enhancement using finite element analysis relies on knowledge of the electrical conductivity and relative permittivity of the elements or compounds in the cable sample. Knowledge of the elemental composition is important in understanding the underlying cause of breakdown since regions with varying permittivity or conductivity can greatly enhance the localized field.

The EDAX Evo 50 SEM system used in the present investigation also facilitates Energy Dispersive X-ray (EDX) spectroscopy, which allows the elemental composition of materials to be determined. Initial results have indicated that several elements were present within the small number of particles considered. Iron, Magnesium, Aluminum, Silicon, Oxygen, Calcium, Sulphur, Copper and Carbon were found to be present in varying quantities from particle to particle. The differences in elemental composition between particles indicates the material has not been synthesized and is some sort of naturally occurring mined mineral ore. This suggests the presence of a filler material, perhaps Magnesium or Aluminium Oxide, to bulk up the EPR at the manufacturing stage. Whether this is the case for the larger particles such as those shown in the CT scans remains to be investigated, as does the effect of electric field concentration on particles made of such compounds. This will be the subject of future analysis.

4 DISCUSSION

The ultimate goal of the investigation is to diagnose the initial cause of the observed breakdown. Analysis has suggested that high contaminant density, eccentricity of the inner core, or a combination of both may have been responsible. Previous work by the authors [11] has suggested that the combination of field enhancement due to conducting particle contamination and core eccentricity causing reduced insulator thickness, has the potential to enhance the localised field above breakdown strength for an aged insulator. It was shown that a spherical conducting particle could increase the electric field concentration to a maximum of 14.43 kV/mm in the present cable geometry. Reported breakdown strengths of EPR are in the region 30-40 kV/mm [12]–[15], with the probability of breakdown increasing with temperature, ageing time and moisture content. Breakdown strength for EPR has been reported to reduce to around 20 kV/mm for ageing times over 11000 hours and with a moisture content of around 1.4 % and greater [12]. Results of the present study seem to confirm this.

That the cable was operational for 26 years indicates that inherent stress enhancement from particle content and geometric non-uniformity caused degradation of the materials. Over the 26 year operating life, localised degradation likely extended through the EPR until a breach was formed and resulted in complete breakdown.

The cable was manufactured according to British Standard BS6622 [6]. Since tests for contaminants were not a

requirement, this was likely not considered at the time of manufacture. BS6622 does, however, specify minimum insulation thickness requirements. Examination of the standard used at the time of manufacture reveals that the cable does not meet these requirements. A 'minimum average thickness' of 3.4 mm and a 'minimum thickness at a given point' 2.96 mm are specified. Since results show a minimum thickness at the breakdown location of 2.7 mm it must be concluded that this was a factor leading to breakdown.

Other standards on medium voltage cable specification, such as AEIC CS8-07 [16], do specify a maximum permissible contaminant diameter and density per unit volume. Although the cable under inspection was not manufactured according to this standard, if we compare the stated maximum permissible particle diameter of 0.125 mm with the largest particle discovered through X-ray CT scanning (0.310 mm as shown in Fig. 11 (a)), it is clear that the cable would also fail this initial test. Examination of the small insulation sample of Fig. 11 (b) shows that the cable would also have exceeded the maximum permissible particle density requirement as stated in AEIC CS8-07 (1 particle >50 μm per cm3) if manufactured according to this standard rather than BS6622. Chan et al [4] correctly note that standard partial discharge testing of a new cable will only indicate the presence of a contaminant if poor bonding occurs between the particle and the surrounding dielectric, resulting in a gas cavity. Although these particles may remain initially undetected, they can lead to breakdown in the long term through electrical or water treeing. It may also be possible for stored charge on particles to lead to attraction of small reactive species which may exacerbate degradation.

Some standards already specify the application of microscopy on new cable samples [16]. Although this procedure is recommended as it would increase the detection rate of any manufacturing anomalies, the occurrence of non-uniform contaminant density or isolated contaminants means that the method of cutting small insulator sections at random is statistically unlikely to yield useful results. Unfortunately, only a single contaminant large enough to induce electric field stressing sufficient to initiate PD or initial tree growth is needed to initiate breakdown of an entire cable section. X-ray methods such as those outlined in the present investigation are effective in detecting such contaminants, but application of the technique on a large scale at the manufacturing stage would be uneconomical and labor intensive. To ensure extruded shielded cable reaches an operational lifespan more closely matching its designed value, it is therefore clear that, in addition to stringent testing requirements, more rigorous contaminant removal processes, such as those discussed in [17]–[19], should be employed at the manufacturing stage. Although strong bonding of contaminants to the surrounding dielectric may preclude *de novo* PD monitoring as a detection strategy, it is proposed that PD detection conducted at least on a regular basis, if not continuously, may lead to successful detection of the effects of particle contamination as the cable ages. This could be tested through the implementation of monitoring strategies on remaining specimens in this family of cables. In addition, future work on finite element modelling and testing of the breakdown strength of contaminated insulation material in light of the present results should contribute to cumulative research towards specifying acceptable limits on the nature and levels of contaminants in extruded dielectric cable systems.

5 CONCLUSIONS

This study has presented the results of an investigation into a defective 11 kV shielded EPR power cable. Breakdown of the defective region was repeated by applying an ac voltage between core and sheath. The fault was then successfully pinpointed using time-difference-of-arrival techniques to isolate the origin of the breakdown pulse to within a few meters. The location of this shunt resistance fault was confirmed to within a few cm using thermal imaging techniques to identify the high temperature region produced by Joule heating of the low resistance fault channel when a voltage was applied to the cable.

Subsequent X-ray analysis of the breakdown region and concomitant through scanning electron microscopy of the surrounding EPR dielectric has suggested a possible cause of breakdown to be degradation initiated by high field stressing due to particle contaminants in combination with an reduced insulation gap due to core eccentricity. X-ray computed tomography has shown the presence of numerous high density particles embedded in the dielectric layer. The maximum contaminant diameter in the region under examination was 310 μm and the average contaminant density was 1 particles per 2.28 mm^3. The minimum insulation thickness in the breakdown region was found to fall below the minimum acceptable value specified in the BS6622 standard, and although no requirement for allowable contaminant levels was specified in this standard, comparison with similar standards, which do specify a minimum contaminant diameter, shows that the cable would have failed in this regard also.

Scanning electron microscopy and energy dispersive X-ray spectroscopy have shown the particle geometry in detail and suggested the elemental composition of the contaminants consists of a metal-oxide ore filler material. In light of these results, it is suggested that operators of cables in the same family adopt a partial discharge monitoring strategy as this may increase the probability of detecting the observed fault in the initial stages of degradation.

Future work will comprise of additional scans of the EPR region. Further studies will be carried out to simulate electric field stressing due to particle contaminants using geometry and elemental composition based in the above results.

ACKNOWLEDGEMENT

This research was funded by the EPSRC through grants EP/G029210/1 (University of Strathclyde) and EP/G028397/1

(Glasgow Caledonian University). The authors would like to thank Dr. Vassilis Charissis for use of Glasgow Caledonian University's Virtual Reality and Simulation laboratory and Dr Mahesh Uttamlal for use of Glasgow Caledonian University's Scanning Electron Microscopy facilities.

REFERENCES

[1] L. Renforth, R. Mackinlay and M. Michel, "MV cable diagnostics - applying online PD testing and monitoring," in Proc. MNC-CIRED Asia Pacific Conference on MV Power Cable Technologies, September 2005.

[2] H. E. Orton, "Diagnostic testing of in-situ power cables: An overview," in Proc. Asia Pacific Transmission and Distribution Conference and Exhibition. Yokohama, Japan: IEEE/PES, October 2002, pp. 1420–1425.

[3] S. Boggs and J. Densley, "Fundamentals of partial discharge in the context of field cable testing," IEEE Electrical Insulation Magazine, vol. 16, no. 5, pp. 13–18, September/October 2000.

[4] J. C. Chan, P. Duffy, L. J. Hiivala, and J. Wasik, "Partial discharge VII: PD testing of solid dielectric cable," IEEE Electrical Insulation Magazine, vol. 7, no. 5, pp. 9–16, Sep–Oct 1991.

[5] B. Clegg, "Underground Cable Fault Location". McGraw Hill Book Company Europe, 1993.

[6] British Standard BS6622: Specification for cables with extruded crosslinked polyethylene or ethylene propylene rubber insulation for rated voltages from 3800/6600 V up to 19000/33000 V. London, UK: British Standards Institution (BSI), 1985.

[7] L. J. Lewis, "Traveling wave relations applicable to power-system fault locators," Trans. American Institute of Electrical Engineers, vol. 70, no. 2, pp. 1671–1680, July 1951.

[8] A. O. Ibe and B. J. Cory, "A travelling wave-based fault locator for two- and three-terminal networks," IEEE Trans. Power Delivery, vol. 1, no. 2, pp. 283–288, April 1986.

[9] P. F. Gale, P. A. Crossley, B. Xu, Y. Ge, B. J. Cory, and J. R. G. Barker, "Fault location based on traveling waves," in Proc. 5th International Conference on Developments in Power System Protection, York, UK, Mar-Apr 1993, p. 54.

[10] Z. Q. Bo, G. Weller, and M. A. Redfern, "Accurate fault location technique for distribution system using fault-generated high-frequency transient voltage signals," IEE Proc. Generation, Transmission and Distribution, vol. 146, no. 1, pp. 73–79, Jan 1999.

[11] A. J. Reid, X.Hu, and M. D. Judd and W. H Siew, "Defect investigation in medium-voltage EPR cable," in Proc. IEEE International Symposium on Electrical Insulation, San Juan, Puerto Rico, 10-13 June 2012.

[12] S. V. Nikolajevic, "The behavior of water in XLPE and EPR cables and its influence on the electric characteristics of insulation," IEEE Transactions on Power Delivery, vol. 14, no. 1, pp. 39–45, January 1999.

[13] M. A. Dakka, A. Bulinski, and S. Bamji, "Correlation between DC polarization and failure characteristics of XLPE and EPR aged with ac voltage in a wet environment," IEEE Transactions on Dielectrics and Electrical Insulation, vol. 12, no. 4, pp. 700–708, August 2005.

[14] J. C. Chan, M. D. Havtley, and L. J. Hiivala, "Performance characteristics of XLPE versus EPR as insulation for high voltage cables," IEEE Electrical Insulation Magazine, Vol. 9, No. 3, pp. 8-12, May-June 1993.

[15] G. Bahder, M. Sosnowski, C. Katz, R. Eaton, and K. Klein, "Electrical breakdown characteristics and testing of high voltage XLPE and EPR insulated cables," IEEE Transactions on Power Apparatus and Systems, vol. PAS-102, no. 7, pp. 2173–2185, July 1983.

[16] "Specification for Extruded Dielectric Shielded Power Cables Rated 5 through 46 kV", 3rd ed. Association of Edison Illuminating Companies (AEIC), 2007.

[17] S. Shinoda, K. Hikino, and M. Marumo, "275kV XLPE insulated aluminum sheathed power cable for Okuyahagi No.2 power station," IEEE Transactions on Power Apparatus and Systems, vol. PAS-100, no. 3, pp. 1298–1306, March 1981.

[18] E. J. McMahon, "A tree growth inhibiting insulation for power cable," IEEE Transactions on Electrical Insulation, vol. EI-16, no. 4, pp. 304–318, August 1981.

[19] B. Yoda, C. Ikeda, Y. Sekii, and M. Kanaoka, "Development of 500 kV cross-linked polyethylene insulated power cable," IEEE Transaction on Power Apparatus and Systems, vol. PAS-104, no. 1, pp. 32–38, January 1985.

Alistair J. Reid (M'11) graduated from the University of Strathclyde, UK, in 2004 with a B.Eng. (Hons) degree in Electrical and Mechanical Engineering and received the Ph.D. degree in 2007 for research on partial discharge monitoring. He conducted post-doctoral research within the Institute for Energy and Environment at the University of Strathclyde, from 2007-2011, studying advanced radiometric techniques for partial discharge detection and diagnostics on underground power cables. He is presently a Research Fellow within the School of Engineering and Built Environment at Glasgow Caledonian University. Alistair is a Member of both the IET and IEEE.

Martin D. Judd (M'02-SM'04) was born in Salford, England, in 1963. He graduated from the University of Hull in 1985 with a B.Sc. (Hons) degree in electronic engineering. His employment experience includes four years working for Marconi Electronic Devices Ltd followed by four years with EEV Ltd, both in Lincoln, England. Martin received the Ph.D. degree from the University of Strathclyde in 1996 for his research into the excitation of UHF signals by partial discharges in gas insulated switchgear. From 1999 to 2004 he held an EPSRC Advanced Research Fellowship concerned with electrodynamics of electrical discharge phenomena. His fields of interest include high frequency electromagnetics, generation and measurement of fast transients, and partial discharges and energy harvesting. Dr. Judd is a Reader in the Institute for Energy and Environment at the University of Strathclyde. He is a Chartered Engineer, a Member of the IET and Senior Member of the IEEE.

Wah Hoon Siew received the B.Sc. (Hons.) degree in electronic and electrical engineering, the Ph.D. degree in electrical engineering in 1982; and the Master of Business Administration degree from the University of Strathclyde, Glasgow, U.K., in 1978, 1982, and 1985, respectively. Currently, he is a Reader in the Department of Electronic and Electrical Engineering at the University of Strathclyde, Glasgow, U.K. His research interests include lightning protection to aircraft and grounded structures, electromagnetic compatibility in large installations due to switching and lightning, lightning, EMP and ESD; and cable diagnostics. Dr. Siew is a Chartered Engineer and a member of the Institution of Engineering and Technology. He is also a member of several CIGRE Working Groups under C4 and a member of the Technical Panel for the IET Professional Network on electromagnetics.

Chengke Zhou (M'07) received the B.Sc. and M.Sc. degrees in electrical engineering from Hua Zhong University of Science and Technology, China in 1983 and 1986, respectively, and the Ph.D. degree at the University of Manchester U.K., in 1994. Since then, he worked in Glasgow Caledonian University, U.K., as a Lecturer, Senior Lecturer and in Heriot-Watt University as a Reader until 2007 when he went back to Glasgow Caledonian University as a Professor. He has published more than 100 papers in the area of partial discharge based condition monitoring of MV/HV plant and power system analysis.

Donald Hepburn (M'08) is a Senior Lecturer in the School of Engineering and Built Environment at Glasgow Caledonian University (GCU). He has been involved in insulation materials research and in partial discharge diagnostics for HV and MV system components for over 19 years. He is a member of CIGRE Joint Working Group A2-D1.46 on transformer solid insulation diagnostics and of the Universities High Voltage network (UHVnet) within the UK. He holds a B.A. (hons) degree from the Open University and a Ph.D. from GCU. Dr Hepburn is a Chartered Engineer, a Member of the IEEE, a Member of the IET and a Member of the Institute of Physics.